# Correctness and robustness of 3D rigid matching with bounded sensor error

Xavier Pennec

INSTITUT NATIONAL DE RECHERCHE EN INFORMATIQUE ET EN AUTOMATIQUE

# *Correctness and Robustness of 3D Rigid Matching with Bounded Sensor Error*

Xavier PENNEC

**N° 2111**

Novembre 1993

PROGRAMME 4

Robotique,
image
et vision


ISSN 0249-6399

INRIA
SOPHIA ANTIPOLIS

# Correctness and Robustness of 3D Rigid Matching with Bounded Sensor Error

Xavier PENNEC

Programme 4 — Robotique, image et vision
Projet Epidaure

Rapport de recherche n° 2111 — Novembre 1993 — 36 pages

**Abstract:** We present in this paper a precise study of Alignment and Geometric Hashing for the recognition of 3D rigid objects in the presence of uncertainty. Given a bounded error on point features, we propagate it through the computations to determine the translation and rotation error. This allows the computation of the compatibility zone, either in the image or in the hash table, to insure the correctness of the algorithm, i.e. the absence of false negatives. This work is presented for the least squares and a basis definition methods. We show the equivalence of these two methods and point out the accuracy of the compatibility zones. We also study the robustness of the alignment algorithm in computing the mean number of hypotheses and false positives with uniform random models and scene. Experiments confirm our analysis.

This theoretical study has important practical applications: in Volume Medical Images Analysis, we show that for typical situations, an alignment scheme can achieve 3D registration for an occlusion ratio as large as 80% with a negligible risk of false match (lower than $10^{-5}$).

**Key-words:** Volume Image Processing, 3D Rigid Recognition, 3D Registration, Alignment, Geometric Hashing, Correctness, Compatibility Zones, Robustness.

*(Résumé : tsvp)*

Unité de recherche INRIA Sophia-Antipolis
2004 route des Lucioles, BP 93, 06902 SOPHIA-ANTIPOLIS Cedex (France)
Téléphone : (33) 93 65 77 77 – Télécopie : (33) 93 65 77 65

# Exactitude et Robustesse de la Reconnaissance Rigide 3D avec une Erreur Bornée

**Résumé :** Nous présentons dans cet article une étude précise des algorithmes d'Alignement et de Hachage Géométrique pour la reconnaissance d'objets rigides 3D bruités. Etant donnée une erreur bornée sur les points caractéristiques, nous la propageons dans les calculs pour déterminer l'erreur sur la translation et la rotation. Cela permet le calcul de la zone de compatibilité, soit dans l'image, soit dans la table de hachage, nécessaire pour assurer l'exactitude de l'algorithme, i.e. l'absence de faux négatifs. Ce travail est présenté pour la méthode des moindres carrés et une méthode par définition de base. Nous montrons l'équivalence de ces deux méthodes et nous en examinons la précision. Nous étudions aussi la robustesse de l'algorithme d'Alignement en calculant le nombre moyen de faux positifs avec des modèles et une scène composés de points aléatoires uniformément répartis. Des expériences confirment notre analyse.

Cette étude théorique a d'importantes applications pratiques : en Analyse d'Images Médicales Volumiques, nous montrons que pour des situations typiques, l'algorithme d'Alignement peut recaler des images 3D ayant un taux d'occultation de 80% avec un risque d'erreur négligeable (inférieur à $10^{-5}$).

**Mots-clé :** Traitement d'Images 3D, Reconnaissance Rigide 3D, Recalage 3D, Alignement, Hachage Géométrique, Exactitude, Zones de Compatibilité, Robustesse.

# 1 Introduction

Object recognition is a major task of artificial vision. In most cases, objects are rigid and known in advance and we have to recognize them in cluttered scenes, requiring the model-based recognition algorithms. Assuming objects and scene are represented by sets of interest features (points, lines ...) and their geometric relations (coordinates), the problem is two-fold : on one hand we have to recognize which objects are in the scene and on the other hand where they are placed. We say that an object is recognized if there exists a mapping of the object in the scene that matches a minimum percentage of object features to scene features. Occluded objects presenting less than this minimum will not be recognized.

Among many methods [Gri92], two recent techniques, Geometric Hashing [LW88] and Alignment [HU87, AF86], proved to adapt well to occlusion with a reasonable complexity. Given minimal sets correspondences, one can compute a transformation between the model and the scene. Alignment uses those minimal sets correspondences as hypotheses and verifies them by mapping the model onto the scene and seeking for scene features close to predicted ones. With the same minimal sets, we can define a model basis and a scene basis, both invariant for the considered set of transformations. Geometric hashing uses the fact that other model features have invariant coordinates in the model basis: using a hash table, we can at recognition time retrieve for each scene pair (basis, point) the possible matched model pairs. Accumulating evidences, we directly obtain the most likely model basis and its matches. This can be repeated over all image minimal sets, keeping each time the best matching.

However, to be practical and robust, these methods have to deal with uncertainty in the image features. Indeed, errors in measurement of features arise from different factors along the image processing, ranging from deformations in the vision system and the inherent sampling of the image to inaccuracies in image preprocessings such as filtering or feature extraction. Thus, an alignment system has to know for each predicted feature in which image zone it has to find a supporting image feature. A geometric hashing system must determine the area which must index a (model, basis) pair.

Both for alignment and geometric hashing, if those regions are too large, incorrect matches may be accepted, giving rise to possibly *false positives* (i.e. a conspiration that leads to the false recognition of an object [GH90]), whereas if they are smaller than necessary, correct matches may be missed,

leading to *false negatives* (no recognition when the object is present). In this paper, we use the term *correctness* to qualify the absence of false negatives and *robustness* to qualify the minimization of false positives.

Using these two algorithms, the first work is then to compute the compatibility zones, which are the regions needed to insure correctness. However, even if we know exactly the zones, there may still be false positives caused by random image features appearing in these regions: in fact, only exact data can ensure the absence of false positives since it is equivalent to null volume error zones. An analysis of the expected number of such false positives is often useful to know the quality of the recognition, and can help fixing how much of the model has to be matched to keep this rate low.

In fact, there are two ways of conducting the analysis depending on how we model the error. The bounded error hypothesis assumes that positional error is bounded. Studies under this assumption were initiated for geometric hashing using point features by Lamdan & Wolfson [Wol90] and Grimson & Huttenlocher [GH90] for 2D affine recognition, and extended to 2D recognition under rigid transformations and similarities in [LW91]. A complete and precise study of 2D affine recognition with geometric hashing and alignment was also presented in [GHJ93]. In a more recent work [AG93], Alter presents an analysis of 2D affine recognition using line features with alignment. On the other hand, Gaussian error modeling leads to "probabilistic recognition", and was studied for geometric hashing by Rigoutsos & Hummel [RH91a, RH91b, Rig92, RH93] for 2D similarities and 2D affine recognition using point features. In recent works [Tsa93, SG93] Tsai and Sarachik focus on 2D affine recognition with alignment or using line features.

Concerning medical imaging, we need to deal with volume images such as 3D CAT-scans or MRI [Aya93]. Previous works [GA92, TGMG92, GA93] used a modified geometric hashing on curves and addressed the uncertainty zone problem using an a-posteriori statistical estimation of invariants accuracy. Recent results in feature extraction [Thi93, TG93] show how to extract reliable feature points from 3D surfaces with a sub-voxel precision, and thus open the problem of 3D recognition under rigid transformations with point features.

In the sequel we will focus on recognition by alignment and geometric hashing for 3D rigid transformations and particularly on two methods for computing the rotation and its associated uncertainty zone: one for alignment in section 2.2, and one for geometric hashing in section 2.3; then, in section 2.4, a statistical study will show that our predicted bounds are quite well

suited. Section 3 will focus on robustness of the alignment scheme, for the prediction stage (3.1), and then for the verification stage (3.2). This will lead to the expected number of false positives, and the expected complexity. Last but not least, we will apply in section 4 our theoretical study to the case of volume medical images registration and show that alignment can achieve registration with an occlusion ratio as large as 80% with a probability of false match lower than $10^{-5}$.

# 2 Recognition under 3D rigid transformations

Assuming we are using features points, a 3D rigid transformation has six parameters, but three points are needed to form a minimal set : although a pair of matched points yields 3 equations, the equations provided by another point matching are linked with the previous ones because the distance between two points has to remain invariant. Hence a pair of matches only yields 5 independent equations instead of 6 and a third pair of matched points is needed to compute all the parameters of a rigid transformation.

**Lemma 1** *The minimal set for 3D rigid recognition with point features is composed of three points and the matching of image and model minimal sets is constrained by 3 additional invariants (for example the inter-point distances in each triplet).*

From now on, let $(m_1, m_2, m_3)$ be the three model points composing the model minimal set and $m$ a generic fourth point of the model. Similarly, we will note $(s_1, s_2, s_3)$ and $s$ the different exact image points. Due to measurement errors, we can only access $(\bar{s}_1, \bar{s}_2, \bar{s}_3)$ and $\bar{s}$, the measured values, with

$$\bar{s}_i = s_i + \delta s_i \quad \text{and} \quad \bar{s} = s + \delta s$$

The bounded error assumption assumes that

$$\|\delta s_i\| \leq \varepsilon_p \quad \text{and} \quad \|\delta s\| \leq \varepsilon_p$$

For ease of analysis, we will only use the $L_2$ norm. Bounds with other equivalent norms such as $L_\infty$ or $L_1$ can be obtained using equivalence coefficients (e.g. in 3D, $\|x\|_2 \leq \sqrt{3}\|x\|_\infty$ ).

## 2.1 Error on the additional invariants

We now focus on the three additional invariants constraining the matching between image and model minimal sets : $l_i = \|m_i - m_{i+1[3]}\| \quad (i = 1, 2, 3)$ are such invariants[1]. Because these values are invariant by rigid transformations, we must have $l_i = \|s_i - s_{i+1[3]}\|$ and so the matching is only valid if $\left| \|\bar{s}_i - \bar{s}_{i+1[3]}\| - l_i \right| \leq 2\,\varepsilon_p$.

**Lemma 2** *The distances between two points in the minimal set are three invariants each one with a compatibility zone of radius* $\varepsilon_l = 2\,\varepsilon_p$.

Many methods can be used to take advantage of these three invariants. As far as geometric hashing is concerned, there are simply 3 added dimensions for them in the hash-table. For alignment, we can use constrained search ([Gri92]) or a simple hashing.

## 2.2 Compatibility zone for alignment

### 2.2.1 Finding the transformation between model and scene minimal sets

Assuming a model minimal set $(m_1, m_2, m_3)$ is associated to an image minimal set $(\bar{s}_1, \bar{s}_2, \bar{s}_3)$, we have to find the rigid transformation mapping the model onto the scene. But due to measurement errors, it is very unlikely that any rigid transformation exactly maps the minimal sets. Hence we choose this transformation by a least squares method.

The translation part of the transformation can be represented by the choices of a model origin $O_m$ and a scene origin $\bar{O}_s$. Let $\bar{R}$ be the rotational part (rotation matrix). The generic transformation of a model point $m$ is :

$$s_{pred} = \bar{O}_s + \bar{R}(m - O_m)$$

Thus, we want to find $(O_m, \bar{O}_s)$ and $\bar{R}$ minimizing the mapping error between the transformed model minimal set and the image minimal set. With a least squares method, they minimize the criterion

$$C = \sum_{i=1}^{3} \|\bar{s}_i - \bar{O}_s - \bar{R}(m_i - O_m)\|^2$$

[1] [3] is module 3.

As far as translation is concerned, the derivation of the criterion easily shows that the origins can be taken equal to the barycenter of each minimal set

$$O_m = \frac{1}{3}(m_1 + m_2 + m_3) \qquad \bar{O}_s = \frac{1}{3}(\bar{s}_1 + \bar{s}_2 + \bar{s}_3)$$

These origins being fixed, we will now work in barycentric frames : let $(x_1, x_2, x_3)$ and $x$ be the barycentric coordinates of the model points ($x_i = m_i - O_m$), $(\bar{y}_1, \bar{y}_2, \bar{y}_3)$ and $\bar{y}$ those of the scene ones ($\bar{y}_i = \bar{s}_i - \bar{O}_s$). The rotation must therefore minimize the criterion

$$C = \sum_{i=1}^{3} \|\bar{y}_i - \bar{R}\, x_i\|$$

Unfortunately, we have no analytical solution, but we dispose of a numerical resolution using quaternions (see [Aya91]) which is developed in appendix A.

### 2.2.2 Compatibility zone for another model point

Assuming the model and scene minimal sets are well associated, there exists a scene origin $O_s = \frac{1}{3}(s_1 + s_2 + s_3)$ and a rotation matrix R mapping exactly the model minimal set to the exact scene minimal set : $s_i = O_s + R(m_i - O_m)$. The exact scene point corresponding to a fourth model point $m$ will then be in $s = O_s + R(m - O_m)$ and will be measured in $\bar{s} = s + \delta s$.
On the other hand, the predicted position of this scene point is given by $s_{pred} = \bar{O}_s + \bar{R}(m - O_m)$. Hence, we have $\bar{s} = s_{pred} + \delta s - \delta O_s + \delta R\,(m - O_m)$ and using barycentric coordinates $\bar{s} = s_{pred} + \delta y + \delta R\, x$. Therefore, the observed point $\bar{s}$ corresponding to the model point $m$ can be found in an volume of radius

$$\varepsilon_{al} = \max \|\delta y + \delta R\, x\| \leq \max \|\delta y\| + (\max \|\delta R\|)\|x\|$$

around the predicted point $s_{pred}$.
The bounded error assumption assumes that $\|\delta O_s\| \leq \varepsilon_p$, so $\|\delta y\| \leq 2\ \varepsilon_p$. Note that our zone only includes the real compatibility zone since we overestimates it. The key problem in this analysis is the determination of the rotational error $\|\delta R\| = \|\bar{R} - R\|$ : we demonstrate in appendix B.1 that,

using barycentric coordinates:

$$\|\delta R\| \leq \frac{4\,\varepsilon_p}{3}\sqrt{\theta_1^2+\theta_2^2} + O(\theta^2) \quad \text{with} \quad \begin{cases} \theta_1 = \dfrac{\sum_{i<j} \|x_i - x_j\|}{3\,\|x_{1\wedge}x_2\|} \\ \\ \theta_2 = \dfrac{\sum \|x_i\|}{\sum \|x_i\|^2} \end{cases}$$

**Theorem 1** *Assuming that a model and a scene minimal set have been matched, the scene point $\bar{s}$ corresponding to a model point $x$ in barycentric coordinates cannot be outside an area of radius*

$$\varepsilon_{al} = 2\,\varepsilon_p(1 + \frac{2}{3}\sqrt{\theta_1^2+\theta_2^2}\,\|x\|)$$

*centered at the predicted point $s_{pred} = \bar{O}_s + \bar{R}x$.*

## 2.3 Compatibility zone for geometric hashing

Geometric hashing is very close to alignment but it separates model calculus from scene ones. Assume we have a method for defining an Euclidian basis with each model and scene minimal set. Taking a fourth model point, alignment projects it in the scene and looks for a scene point there (or around when error is taken into account). Instead, Geometric hashing computes its coordinates in the model basis and says that a scene point with these coordinates in the scene basis can be matched. Hence, in a preprocessing stage, we just have to compute the coordinates of every model point in each basis defined by a model minimal set and index that basis with those coordinates. At recognition time, we choose a scene minimal set, compute the coordinates of every scene point in the associated basis and accumulate through the hash-table evidences of matching for every model basis. In fact, we can collapse every model in the hash-table, making the recognition time almost independent of the number of models (for a more detailed description of the algorithm see [LW88, LW91]). In our case, for 3D rigid recognition, we will add 3 dimensions in the hash-table indexing the 3 additional invariants for the chosen minimal set.

### 2.3.1 Defining a basis from a minimal set

We would like to find a definition that leads to the same transformation as with the least squares method. Hence, we already know that the origin must be taken equal to the barycenter. Corollary 1 of appendix A.5 shows us that the least squares rotation superimposes axes orthogonal to the two triplets of points. Therefore we can choose an axis orthogonal to the plane defined by the minimal set. To define an Euclidian basis, we still have to choose another axis in this very plane, the third one being automatically defined as orthogonal to the others. It seems difficult to choose such an axis leading to the same transformation as with the least-squares method. Thus, we choose the most stable axis in the minimal set : the one defined by the two points of maximal distance (see figure 1). To avoid orientation problems, we sort the three points $(a, b, c)$ such as $\|b-a\| \geq \|c-b\| \geq \|c-a\|$. The definition of the basis is therefore

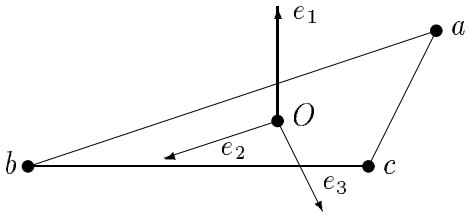


Figure 1: Definition of a basis from a minimal set.

$$\mathcal{B}(a,b,c) = \left( O = \frac{a+b+c}{3} \; ; \; e_1 = \frac{(a-O)\wedge(b-O)}{\|(a-O)\wedge(b-O)\|} \; ; \; e_2 = \frac{b-a}{\|b-a\|} \; ; \; e_3 = e_1 \wedge e_2 \right)$$

Since equalities can holds in the orientation convention, there can be several possible bases. Hence, a great care has to be taken in the preprocessing stage: if two or even three distances between the three points are compatible (i.e. equal up to $\varepsilon_l = 2\,\varepsilon_p$), one has then to index the different possible bases. With this precaution, we have no extra care to take at recognition time.

### 2.3.2 Compatibility zone in invariant coordinates space

Let $\mathcal{R}(a,b,c)$ be the rotation matrix $\mathcal{R} = [e_1, e_2, e_3]$. To compute the coordinates of a point $p$ in the basis we have defined, we just have to solve the system $p = O + \mathcal{R}x$.

In the preprocessing stage, we define the basis from the minimal set $(m_1, m_2, m_3)$, get the origin $O_m$ and the rotation $R_{prep} = \mathcal{R}(m_1, m_2, m_3)$. A model point m is then indexed by the location

$$x = R_{prep}^{-1}(m - O_m)$$

Assuming we have perfect models, this can be done without error. At recognition time, we solve in fact

$$(R_{rec} + \delta R_{rec})(x + \delta x) = s + \delta s - O_s - \delta O_s$$

Assuming the real location of the point $s$ in invariant space is given by $R_{rec}x = s - O_s$ and using barycentric coordinates, we find

$$\delta x = (\bar{R}_{rec})^{-1}(\delta y - \delta R_{rec}\, x)$$

Taking a bound on it we have

$$\|\delta x\| \leq \|\bar{R}_{rec}^{-1}\| \, (\|\delta y\| + \|\delta R_{rec}\| \, \|x\|)$$

Once again the bounded error assumption ensures that $\|\delta y\| \leq 2\, \varepsilon_p$, and since $\bar{R}_{rec}$ is a rotation, $\|\bar{R}_{rec}^{-1}\| = 1$. On the other hand, we demonstrate in appendix B.2 that, using barycentric coordinates:

$$\|\delta R_{rec}\| \leq \frac{4\, \varepsilon_p}{3} \sqrt{\theta_1^2 + \theta_{2'}^2} + O(\theta^2) \quad \text{with} \quad \begin{cases} \theta_1 = \dfrac{\sum_{i<j} \|x_i - x_j\|}{3\, \|x_{1\wedge} x_2\|} \\ \\ \theta_{2'} = \dfrac{3}{2\ \max_{i,j} \|x_i - x_j\|} \end{cases}$$

**Theorem 2** *In the three dimensional space of invariant coordinates (subspace of the hash table), a point located at $x$ has a maximum error in norm of*

$$\varepsilon_{gh} = 2\, \varepsilon_p \left(1 + \frac{2}{3} \|x\| \sqrt{\theta_1^2 + \theta_{2'}^2}\right)$$

## 2.4 Validity and validation of rotational bounds

The formulation of the two bounds being rather complex, principally due to the rotational part, it is interesting to know what they really mean, i.e. what are the geometric parameters implicated, and up to what values of those parameters we can keep a good confidence. This will help us choosing the minimal set by confirming heuristics or on the contrary discarding certain minimal sets as degenerated because of the error. A second important question is how large or tight our bounds are, and how representative of the maximal error they are. For the sake of simplicity, we will only be concerned with the rotational error.

### 2.4.1 Analysis of formulas and domain of validity

Let $(x_1, x_2, x_3)$ be the model basis (minimal set) in barycentric frame. This triplet forms a triangle whose characteristics are (amidst others)

- *Perimeter* $p = \sum_{i<j} \|x_i - x_j\|$
- *Surface* $\mathcal{S} = \frac{1}{2}\|(x_1 - x_2)_\wedge(x_1 - x_3)\| = \frac{3}{2}\|x_{1\wedge}x_2\|$

Let $r$ be the radius of the basis inscribed circle. We can see that ([Ber92])

$$\theta_1 = \frac{p}{2\,\mathcal{S}} = \frac{1}{r}$$

Moreover, the definition of $r$ implies that $r < \|x_i\|$ and hence

$$\theta_2 = (\sum \|x_i\|)/(\sum \|x_i\|^2) < \theta_1$$

Similarly, since $\|x_i - x_j\| > 2r$, we get $\theta_{2'} = 3/(2 \max \|x_i - x_j\|) < \theta_1$. Taking this into account, we shall overestimate the rotational error by

$$\|\delta R\| < \frac{4\sqrt{2}}{3}\frac{\varepsilon_p}{r}$$

and hence the ration $r/\varepsilon_p$ can be considered as the precision of the rotation.

Therefore, we know that $\theta_1$ is the dominating term, and the validity of the formulas is given by $\varepsilon_p \ll r$. However, it is unclear whether $\theta_1$ dominates strongly or not. We draw in figure 2 this error with the convention that the edge of maximum length is $(x_1, x_2)$. We also take this length for unit measure. Hence, the error is drawn in $Z$-axis in function of the position of the third

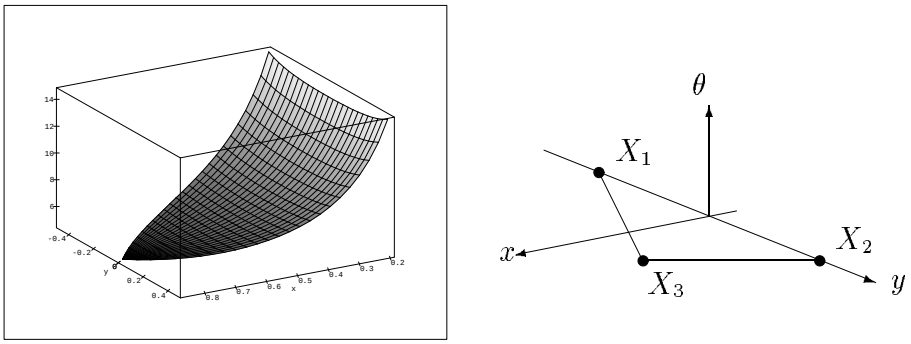


Figure 2: Error $\frac{4\,\theta_1}{3}$ and position of the minimal set points.

point $x_3$ inside an equilateral triangle. We do not present the total error since for both methods the graphics are similar : as a result, $\theta_2$ only perform a very small vertical shift.

A second point is that the basis definition method appears to be slightly better than the least squares one. Actually, this has to be moderated by the very small relative difference shown by figure 3.

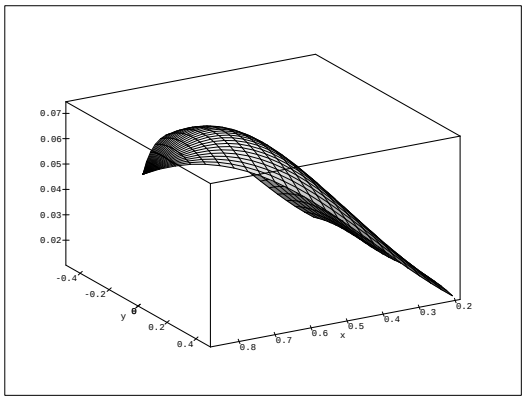

Figure 3: Relative error $\frac{\|\delta R\| - \|\delta R_{rec}\|}{\|\delta R\|}$ between the two methods.

Last but not least, the minimum error is obtained for the equilateral triangle, which seems rather coherent. Hence we can conclude these two methods are more or less equivalent, the principal parameter of the error being $1/r$ where $r$ is the radius of the basis inscribed circle.

### 2.4.2 Accuracy of the bounds : statistical study

To be practical, we need to know the accuracy of our bounds. The aim of this study is to characterize the real distribution of error relatively to the predicted bound. Therefore, we have to separate the different parameters into two classes : those which affect the predicted bound, and those which do not, upon which we will compute our distribution of error.

Clearly, the computed bound $\|\delta R\|$ or $\|\delta R_{rec}\|$ only depends on the position of the model basis and the error bound $\varepsilon_p$. Other parameters, such as the error on the basis points or the position $x$ of the point to be processed, belong to the second class. Actually, we are interested in the distribution of $\|\delta R\, x\|$ for a fixed pair (basis, $\varepsilon_p$), but since this is linear in $\|x\|$, we can focus on $\|\delta R\, x\|/\|x\|$.

We therefore choose 400 random pairs (basis,$\varepsilon_p$), assuming only that $\varepsilon_p < r/10$ to avoid degenerated bases. For each pair, we compute the predicted bound $\|\delta R\|$ which acts as the abscissa on our graph. Then we disturb 1000 times the basis with a uniform random error bounded by $\varepsilon_p$ on each basis point and for each disturbance we compute the error $\|\delta R\, x\|/\|x\|$ for 500 random points $x$ (uniform law). We thus obtain a population of 500 000 values of the rotational error and we choose to characterize this population by its mean and maximum values. These values are the ordinates on the graph.

- **The least squares method**
  The first observation on the graph plotted in figure 4 is the compactness of the mean error distribution around a line. Computing the regression line, we got
  $$\text{mean error} = \frac{\text{predicted error}}{13.2}$$
  As far as the maximum error is concerned, which is actually what we were tempting to bound, we observe a sparse distribution. this seems rather natural since the maximum of a population is not very stable. Calling *max* this statistic, we shall however note that
  $$\frac{\text{max}_{pred}}{5.5} \leq \text{max} \leq \frac{\text{max}_{pred}}{2}$$

- **the basis-definition method**
  The graph is so similar to the least squares one that it is virtually indistinguishable. The only difference which can be noted is the regression

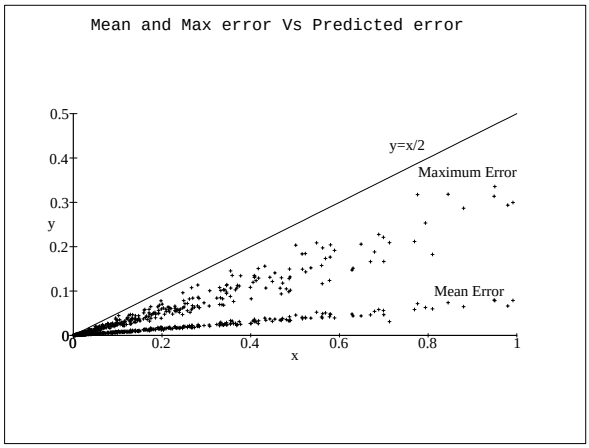


Figure 4: Mean and maximum error versus predicted error bound with the least squares method

line on mean error :

$$\text{mean error} = \frac{\text{predicted error}}{12.9}$$

This statistical study therefore achieves to convincing that the two methods are equivalent. Moreover, it proves that our bounds are quite well suited.

## 2.5 Practical use of the bounds

Up to here, we developed a method which avoids all false negatives. The major drawback of taking a bound on the error into account is the rapid growth of the false positives with the size of the error zone. A trade-off has then to be realized between the two extremes. The statistics of section 2.4.2 suggest that the error law is linear with respect to the predicted bound. The idea is then to use an adjustment coefficient on the predicted bound. In order to do that, we draw in figure 5 an abacus indicating the rate of points outside the error zone as a function of the adjustment coefficient. If for instance we are looking for a recognition with 50% of the model points, we can allow 1 point upon 100 to be "forgotten" (leading to a 49% recognition) and then thus divide the radius of our error zone by five.

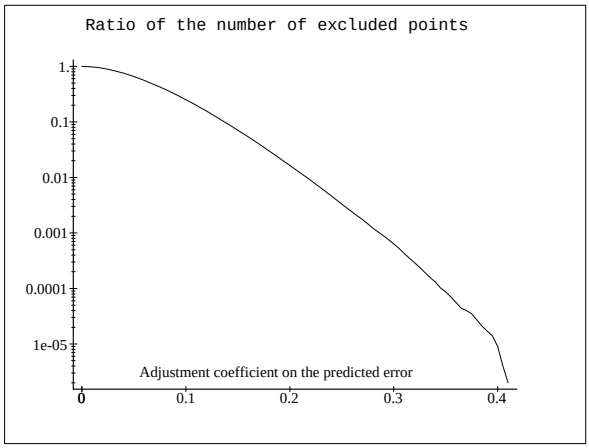


Figure 5: Ratio of the number of points lying outside of an adjusted error zone (weighted by the coefficient in abscissa). The statistics are realized using 200 random bases, 500 disturbances per basis and 200 points per disturbances.

# 3 Robustness in the presence of noise

In the previous section, we focused on building error zones for alignment and geometric hashing, leading to correctness: using those compatibility zones, we are certain to avoid false negatives. But the question is now how robust such methods are. We will use for this section the least squares method, but having shown that the basis definition method is equivalent, the analysis will also holds for it.

The aim of this part is the analysis of the algorithms to determine what is the probability of recognizing a model in a random scene. In fact, for our applications, we will only be concerned with the alignment scheme because it will appear to be the best trade-off between complexity in time and complexity in memory. In a first step, we will analyze the prediction stage of the algorithm and show that it can be very powerful. The analysis of the verification stage will then allow us to conclude on the expected number of false positives (false recognitions), and on the induced consequences.

For the analysis, we consider a collection of $M$ models of $m$ points each, and a scene of $n$ points. We assume a uniform distribution of the scene points over the image, and also a uniform distribution of the model points. For the sake of simplicity, we will call 'basis' a minimal set.

## 3.1 Prediction stage

### 3.1.1 The hashing scheme

Before mapping the model onto the scene, we have to predict the matching between a model and a scene basis. We saw that in our case this is constrained by three additional invariants, which we chose to be the inter-point distance in the basis. With the orientation convention of section 2.3.1, the three distances are ordered such that $d_1 < d_2 < d_2$. As in the basis definition method, the uniqueness of this orientation splits into several cases (a small number however) if two or even three distances are compatible.

Let $\mathcal{M} = (m_1, m_2, m_3)$ be a model basis and $q_1 = (d_1, d_2, d_3)$ its vector of invariants. A scene basis $\mathcal{S} = (s_1, s_2, s_3)$ with vector of invariants $q_2$ is compatible with $\mathcal{M}$ if $\|q_2 - q_1\|_\infty \leq \varepsilon_l = 2\,\varepsilon_p$. To take advantage of the additional invariants, we build in a preprocessing stage a hash table indexing every possible model basis from its vector of invariants and the associated error zone (there are $\binom{m}{3}$ such bases). At prediction time, we just have to choose an image basis and retrieve through the hash table the compatible model bases: we directly have the hypotheses to be validated in the verification stage. We are now focusing on the average number of model bases compatible with one image basis, and the average number of hypotheses to be verified.

### 3.1.2 Error Analysis

For the sake of simplicity, let the dimension of the model and scene images be $1 \times 1 \times 1$ and let $d$ be the scale factor. To determine the expected number of model bases compatible with a random scene basis, we first need to know the expected *spread* of an entry, which is the mean probability of indexing one model minimal set.

- **Mean spread**
  Let $\rho(q)$ be the probability density of a vector of invariants $q$ induced by a uniform probability over the image for each points of the basis. A vector of invariants $q_r$ is compatible with the vector of invariants $q_i$ of the hash table if $q_r = q_i + q$ with $\|q\|_\infty \leq \varepsilon_l / d$. Hence the probability of indexing $q_i$ is given by

$$p(q_i) = \int_{\|q\|_\infty \leq \frac{\varepsilon_l}{d}} \rho(q_i + q)\, dq$$

Developing $\rho$ to the first order, and neglecting boundary conditions, we obtain

$$p(q_i) = \left(\frac{2\,\varepsilon_l}{d}\right)^3 \rho(q_i) + O\left(\left(\frac{\varepsilon_l}{d}\right)^5\right)$$

The mean spread $\mu_H$ is defined by the expected value of $p$ over the $q_i$'s in the hash table:

$$\mu_H = E(p) = \int_H p(q)\rho(q)dq = \left(\frac{2\,\varepsilon_l}{d}\right)^3 I + O\left(\left(\frac{\varepsilon_l}{d}\right)^5\right)$$

with $\quad I = \int_H \rho(q)^2 dq$

- **Ideal hash table**
  In this case, the probability density $\rho(q)$ would be uniform over the hash table. Let $V_H$ be the volume of the hash table:

$$\hat{I} = \int_H \frac{dq}{V_H^2} = \frac{1}{V_H}$$

  Taking three distances[2] $d_1 \leq d_2 \leq d_3 \leq \sqrt{3}$, they can be derived from a triangle only if $d_3 < d_1 + d_2$. These equations define a tetrahedron whose volume is $\sqrt{3}/4$. Therefore, a first estimation is $\quad \hat{I} = 4/\sqrt{3} \simeq 2.31$.

- **Statistical estimation**
  We compute an histogram of the positions of $q$ in the hash table, and integrate the square of this estimation of $\rho$, the three points composing the basis following a uniform distribution over the image. With a cell volume of $(\sqrt{3}/200)^3 = 6.7\,10^{-7}$ and a sample of size $n = 10^8$ we obtain $\hat{I} = 8.805$.

- **Mean number of model bases indexed by one scene basis**
  Let $\beta = M\binom{m}{k}$ be the number of indexed bases in the hash table, and $\mu_H$ the mean spread of each entry. By definition, $\mu_H$ is the probability that a vector of invariants indexes one basis through the hash table. Hence, the probability that this vector indexes $j$ points follows the binomial distribution $B_{(\beta,\mu_H)}(j)$ and the mean number of indexed basis is

$$N_{mod} = \beta\,\mu_H = I\,\left(\frac{4\,\varepsilon_p}{d}\right)^3 M\binom{m}{3}$$

[2]The maximum distance between two points in a cubic image of dimension 1 is $\sqrt{3}$.

### 3.1.3 Experimentations

To check the correctness of our analysis, we computed a random model image of dimension $d = 128$ with $m = 25$ and 50 points and built the hash table for three values of $\varepsilon_p$ : 1,2 and 4. Then we took an arbitrary scene of the same dimension and number of points and computed the average number of model bases associated with each scene basis. The results are presented in table 1.

In fact, our results show a very good adequacy between the measured values and the prediction with the statistical estimation, and raise the inadequacy of the hypothesis of a uniform hash table. For instance, considering 50 points and an error of $\varepsilon_p = 2$ (boldface numbers in table 1), we obtain an average number of 44.6 model bases matching one image basis while we predicted 42.1 with $I = 8.8$ (and 11 with $I = 2.03$). The slight underestimation we obtain comes from the underestimation of the number of model bases indexed in the hash table : indeed, we count only once the bases those split into several because of the non uniqueness of the orientation convention. Be what it may, the adequacy of the results justifies our hypotheses, and we shall take from now on $I = 8.8$.

Moreover, it shows that the hash table performs a very strong pruning of the possible hypotheses, since, for the same example, 45 model bases are only 0.23% of the 19600 possible model bases.

| m=25 | I=2.31 | I=8.8 | measured |
|---|---|---|---|
| $\varepsilon_p$=1 | 0.162 | 0.618 | 0.677 |
| $\varepsilon_p$=2 | 1.297 | 4.941 | 5.117 |
| $\varepsilon_p$=4 | 10.38 | 39.53 | 38.94 |

| m=50 | I=2.31 | I=8.8 | measured |
|---|---|---|---|
| $\varepsilon_p$=1 | 1.382 | 5.264 | 5.69 |
| $\varepsilon_p$**=2** | **11.05** | **42.11** | **44.65** |
| $\varepsilon_p$=4 | 88.43 | 336.87 | 345.5 |

Table 1: Predicted and measured values of the mean number of model bases compatible with one image basis.

### 3.1.4 Mean number of hypotheses

Let $c$ be the occlusion rate: we can only see $(1-c)m$ points of a model amidst the scene ones. Hence, $\binom{(1-c)m}{3}$ bases among the $\binom{n}{3}$ possible in the scene lead to a correct recognition. Assuming we stop our computations as soon as we find a good solution, we will stop with one of these bases. The probability to chose one of these bases is $r = \binom{(1-c)m}{3} / \binom{n}{3}$ and the probability to find

the first correct basis at step $t$ is $r(1-r)^{(t-1)}$. The mean number of bases to be processed before finding a good one is then the expected value of $t$

$$N_{im} = E(t) = \frac{1}{r} = \frac{\binom{n}{3}}{\binom{(1-c)m}{3}}$$

**Theorem 3** *The mean number of hypotheses produced by the prediction stage for a uniform random scene is*

$$N_{hyp} = N_{mod}\, N_{im} = \hat{I} \left(\frac{4\,\varepsilon_p}{d}\right)^3 \frac{M\binom{m}{3}\binom{n}{3}}{\binom{(1-c)m}{3}}$$

*with* $\hat{I} = 8.8$ *for uniform random models.*

## 3.2 Verification stage

Assuming we have an hypothesis, we are now looking for a confirmation by mapping each model point onto the scene and looking for some scene point in its compatibility zone.

### 3.2.1 Mean spread

For a given model point $m$, we will call *spread* the probability that a random scene point fall in its compatibility zone which is the sphere $\mathcal{S}(s_{pred}, \varepsilon_{al})$. Taking once again an image $1\times1\times1$, this is simply $\mu = \int_{(Image \cap \mathcal{S}(s_{pred}, \varepsilon_{al}))} dx$ . For the sake of simplicity, we will take an overestimation of $\mu$ in neglecting boundary conditions : $\mu = 4/3\pi\varepsilon_{al}^3$. An advantage of this simplification is that we eliminate all dependencies from the scene points, and only keep dependencies from the model points. The expected value of $\mu$ is then

$$\bar{\mu} = E(\mu) = \frac{4\pi}{3} \int \varepsilon_{al}^3(m_1, m_2, m_3, m)$$

Let $J$ be the integral $J = \int (\varepsilon_{al}/2\,\varepsilon_p)^3$. According to theorem 1, and using its notations, we have

$$J = \int \left(1 + \frac{2}{3}\|x\|\sqrt{\theta_1^2 + \theta_2^2}\right)^3$$

However we saw that our bound on the rotational error is only valid when $r$, the radius of the inscribed circle to the basis, is large according to $\varepsilon_p$.

Moreover, small values of $r$ lead to virtually undefined rotations and very huge to infinite error bounds. Hence, we have to eliminate these degenerated bases by fixing an inferior threshold on the acceptable values of $r$: this will moreover assure the convergence of the integral $J$.

The exact computation of $J$ for the acceptable values of $r$ being rather messy, we draw in figure 6 a numerical computation of $J(r_{min})$. A regression on these data gives for approximation

$$\hat{J}(r_{min}) = \frac{4.80}{r_{min}}$$

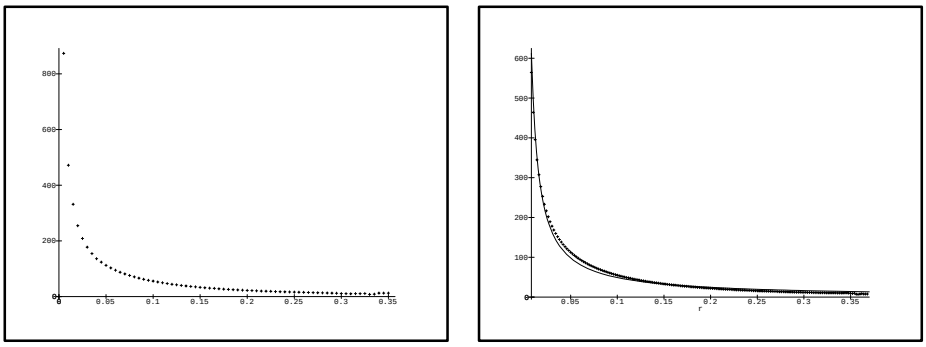

Figure 6: Left : Numerical integration of $J(r_{min})$ with a Monte Carlo sampling of size $10^7$. Right : superimposition with the regression curve $y = 4.80/r_{min}$.

Hence, including the scale factor, we get

**Lemma 3** *The mean spread of a compatibility zone is given by*

$$\bar{\mu} = \frac{4\pi}{3} \left(\frac{2\,\varepsilon_p}{d}\right)^3 J\left(\frac{r_{min}}{d}\right) + O\left(\left(\frac{\varepsilon_p}{d}\right)^5\right)$$

*an approximation of $J$ being* $\hat{J}\left(\frac{r_{min}}{d}\right) = 4.80\,\frac{d}{r_{min}}$

Since $r_{min}$ has to be a bit larger than $\varepsilon_p$, it can be written $r_{min} = \alpha\,\varepsilon_p$ with $1 < \alpha < d/2$ , and the approximated mean spread becomes

$$\hat{\mu} \simeq \frac{161}{\alpha} \left(\frac{\varepsilon_p}{d}\right)^2$$

### 3.2.2 Probability of accepting an hypothesis

When we map the model onto the scene, the probability that one scene point falls in the compatibility zone of one model point is the mean spread $\bar{\mu}$. Since there are $m-3$ such zones, the probability for one scene point to be in at least one of them is $\rho = 1-(1-\bar{\mu})^{m-3}$. Repeating this operation for each of the $n-3$ scene point, the probability of having $j$ matchings follows the binomial law $B_{(m-3,\rho)}(j)$. Let $\tau$ be the acceptance threshold on the number of matched pairs:

**Lemma 4** *The probability of accepting a given hypothesis is*

$$q = \sum_{j \geq \tau} B_{(n-3,\rho)}(j) = \sum_{j=\tau}^{n-3} \binom{j}{n-3} \rho^j (1-\rho)^{n-3-j} = I_\rho(\tau, n-\tau-2)$$

*with* $\rho = 1-(1-\bar{\mu})^{m-3}$, *and* $I_p(a,b)$ *being the incomplete normalized Beta function.*

If $\rho \ll 1$, we can approximate the binomial $B_{(n-3,\rho)}$ with the Poisson law of parameter $\lambda = (n-3)\rho$ and we obtain

$$q \simeq 1 - e^{-\lambda} \sum_{j=0}^{\tau} \frac{\lambda^j}{j!}$$

### 3.2.3 Experimentations

We computed a random model image of dimension $d = 128$ with $m = 25$ and 50 points and built the hash table for $\varepsilon_p = 2$. Then, we computed a sufficient number of scene images of the same dimension to obtain at least $10^6$ hypotheses. For each one, we map the model onto the corresponding scene and compute the histogram of the number of scene points within our error zones. Dividing by the number of hypotheses, we obtain a measure of the probability $q$ of accepting an hypothesis with respect to the variable $\tau$, the acceptance threshold. The results are presented in figure 7.

Once again, these experimentations justify our theoretical analysis: we really obtained an overestimation of $q$ : for example, when we match at least 15 points over 50 with an error $\varepsilon_p = 2$, we predict a probability $q = 8.51\,10^{-3}$ but our experiment shows a value of $1.23\,10^{-4}$.

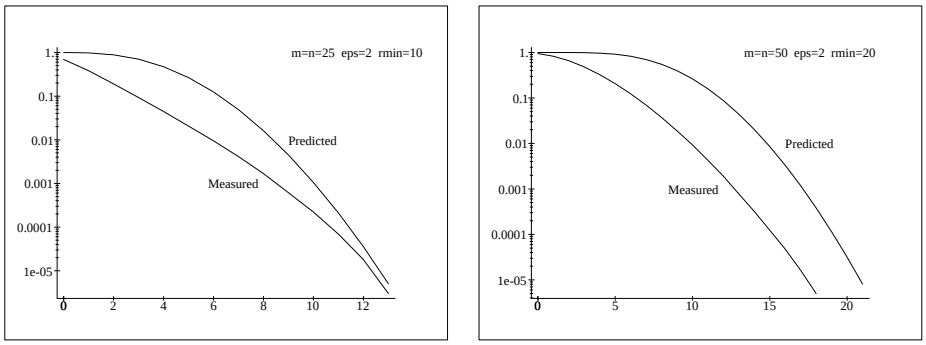


Figure 7: Predicted and measured values of the probability $q(\tau)$ of accepting an hypothesis (logarithmic scale). Left: $m = n = 25$, $\varepsilon_p = 2$, $r_{min} = 10$. Right: $m = n = 50$, $\varepsilon_p = 2$, $r_{min} = 20$.

### 3.2.4 Number of false positives

Since we have $N_{hyp}$ hypotheses to verify, the probability of accepting $j$ hypotheses follows the binomial law $B_{(N_{hyp},q)}(j)$ and the mean number of false positives is $N_{fp} = q\, N_{hyp}$.

This number can be very useful to determine the acceptance threshold $\tau$: keeping the number of false positives under a given value is a good criterion.

**Theorem 4** *The number of false positives is given, with previous notations, by*

$$N_{fp} = \hat{I}\left(\frac{4\,\varepsilon_p}{d}\right)^3 \frac{M\binom{m}{3}\binom{n}{3}}{\binom{(1-c)m}{3}} I_\rho(\tau, n-\tau-2)$$

*with* $\quad \rho = 1-(1-\bar{\mu})^{m-3} \quad$ *and* $\quad \bar{\mu} = \frac{4\pi}{3}\left(\frac{2\,\varepsilon_p}{d}\right)^3 J\left(\frac{r_{min}}{d}\right)$

## 3.3 Expected complexity

In a preprocessing stage, we construct the hash table for every model minimal set in a time $O(Mm^3)$. The prediction stage creates $N_{hyp}$ hypotheses in a time $O(N_{im})$ and each hypothesis has to be verified by mapping each other model point onto the scene and looking for the closest scene point. With a reasonable preprocessing of the scene, this can be done in constant time (see [Dan80]). The verification stage takes then a time $O(m)$ and the overall

complexity of recognition is

$$O\left(Mm^4\left(\frac{n\,\varepsilon_p}{\tau\,d}\right)^3\right)$$

In fact, the real complexity is often dominated by the preprocessing stage.

# 4 Application to medical imaging

The main application of this work in medical imaging concerns rigid registration of 3D images, for instance to compare two images of the same patient taken at different times. In many cases, registration of bones for example, we can assume that the transformation between the images is rigid. In a recent work [Thi93, TB93], J.P. Thirion showed how to extract some reliable and precise feature points, called extremal points, from three-dimensional images such as MRI (Magnetic Resonance images) or Cat-Scan images. With these feature points, we can use many algorithms, and among them alignment or geometric hashing. Here, the characteristics of the application are a number of model $M = 1$ since we are doing registration and a number of points nearly identical in the model and the scene, varying from 100 to 10000. The typical dimension of the images is between $100^3$ and $256^3$ and the magnitude of the positional error on points reaches one voxel. Actually, after registration, the percentage of matched points vary from 15% to 50% (see [TB93]).

In fact, geometric hashing is very hard to use for these applications since we have to create $(m-3)\binom{m}{3} = O(m^4)$ entries in the hash table. If it is feasible for less than a hundred points, it comes rapidly to a very huge amount of memory with our number of points. Therefore, we just use alignment which only needs $\binom{m}{3}$ entries in the hash table.

## 4.1 Theoretical number of false positives

To check the robustness of this algorithm for this particular type of application, we chose several parameters: an image dimension $d = 128$, an error $\varepsilon_p = 1$, and a number of points $m = n$ from 50 to 500 with an occlusion ratio of 70%. Hence, we took $\tau = 0.30\,m - 3$ since 3 points are needed for the minimal set. For the prediction stage, we used the ideal value $\hat{I} = 8.8$, and for the verification stage, the approximation $\hat{J} = 4.80\,d/r_{min}$ with $r_{min} = 10$.

We present the predicted number of associations and false positives in table 8: if no false positive is obtained for a number of points less than about

| $m$ | 50 | 100 | 200 | 300 | 500 |
|---|---|---|---|---|---|
| $N_{hyp}$ | 468 | 2400 | 15831 | 50287 | $2.2\,10^5$ |
| $q$ | $8.4\,10^{-7}$ | $9.4\,10^{-8}$ | $6.12\,10^{-5}$ | $6.6\,10^{-2}$ | 0.999989 |
| $N_{fp}$ | $3.96\,10^{-4}$ | $2.24\,10^{-4}$ | 0.97 | 3344 | $2.2\,10^5$ |

Figure 8: Mean number of bases associations $N_H$, probability of acceptance $q$ and mean number of false positives $N_{fp}$ when matching 30% of the $m$ points. Image $128^3$, error $\varepsilon_p = 1$, $r_{min} = 10$.

200, this is not at all the case for a larger number of points. For 500 points, we even filter nothing since we accept all the hypotheses ($q \simeq 1$). Therefore, we compute in table 2 the minimal value of the acceptance threshold $\tau$ required to keep the number of false positives lower than $10^{-5}$.

| $m$ | 50 | 100 | 200 | 300 | 500 |
|---|---|---|---|---|---|
| $\tau$ | 14 | 30 | 71 | 124 | 250 |
| $(\tau+3)/m$ (%) | 34 % | 33 % | 37 % | 42.3 % | 51% |

Table 2: Minimal value of the acceptance threshold $\tau$ and the corresponding percentage of matched points to keep the number of false positives under $10^{-5}$ (actually $\tau$+3 points are matched since we have to count the minimal set).Image $128^3$, error $\varepsilon_p = 1$, $r_{min} = 10$.

## 4.2 Practical use

In fact, we saw in section 2.4.2 that we could without loss of correctness divide the bound on rotational error by a factor at least two. Including this factor 0.5 in our computations, we recomputed the integral $J$ and obtain an approximation $\hat{J}_{0.5} = 1.20(d/r_{min})$. With this new value, we also recomputed in table 3 the acceptance threshold needed to keep the number of false positives under $10^{-5}$ and we got some very interesting results: for instance, registering two images of dimension $128^3$ and assuming 100 points extracted on each with an error less than $\varepsilon_p = 1$, we only need to match 16 points more the minimal set, that is 19% of the number of points.

With this more adapted use of our formulas, the alignment algorithm appears to be very convenient and powerful for real applications in volume

| $m$ | 50 | 100 | 200 | 300 | 500 |
|---|---|---|---|---|---|
| $\tau$ | 9 | 17 | 34 | 54 | 110 |
| $(\tau+3)/m$ (%) | 24 % | 20 % | 18.5 % | 19 % | 23% |

Table 3: Minimal value of the acceptance threshold $\tau$ and the corresponding percentage of matched points to keep the number of false positives under $10^{-5}$ with a coefficient 0.5 on the rotational error bound.Image $128^3$, error $\varepsilon_p = 1$, $r_{min} = 10$.

image registration. Unlike 2D affine recognition (see [GHJ93]), we do not have to add a supplementary step of verification. Moreover, The hash table used in the prediction step proved to be very powerful since it decreases the prediction step to a constant time. We have hence obtained an ideal tool for volume images registration.

# 5 Conclusion

While focusing on exact recognition algorithms for 3D point features with bounded sensor error, we showed first that the minimal set is composed of three such points and that matching image and model minimal sets is constrained by 3 additional invariants. We used these invariants in a hash table to reduce efficiently the complexity of the prediction stage. We also examined two methods for computing a rigid transformation between two minimal sets: the least squares method and the basis definition one. Both can be used by alignment whereas geometric hashing is restricted to the second. We determined that the compatibility zone centered at the predicted point is actually the same for both methods, the dominating parameter being the radius of the circle inscribed to the minimal set triangle. A threshold on this parameter has to be used to avoid degenerated bases. We also showed that our bound is relatively tight, up to a factor 1/2, and well representative of the maximum error.

The study of the robustness for random model and scene images allowed us to define precisely the domain of validity of our alignment algorithm for volume image registration, and it proved to be very robust to occlusion since we can still recognize with a negligible risk models 80 % occluded.

However, in a future work, we have to adapt the random model we used for model and scene image features to real medical images. Other interesting

points are the analysis and prediction of the accuracy of the registration we obtain, and the addition of supplementary attributes on points.

# 6 Acknowledgments

I want to thank Nicholas Ayache, Jean Philippe Thirion and Jacques Feldmar for stimulating discussions about numbers of 'great ideas' or small details during this work. Part of this work was supported by Digital Equipment Corporation, by the European Basis Research Action Viva (Esprit project) and by a fellowship from D.R.E.T./D.C.N (France).

# A Quaternions and least squares rotation

## A.1 Definition

Quaternions are the elements of a 4 dimensional algebra on $\mathbb{R}$ which we shall note $\mathcal{Q}$. This is also the first non-commutative division ring (skew field) found by Hamilton in 1843. We can construct this algebra in several ways, but the one we will be interested in considers a quaternion $q \in \mathcal{Q}$ as a pair $q = (a, v)$, where $a \in \mathbb{R}$ is the real part and $v \in \mathbb{R}^3$ the so-called pure part. The operations defined on quaternions to form the algebra are :

- Addition : $(a_1, v_1) + (a_2, v_2) = (a_1 + a_2, v_1 + v_2)$
- Internal multiplication : $(a_1, v_1) * (a_2, v_2) = (a_1 a_2 - < v_1 | v_2 >, v_{1\wedge} v_2 + a_1 v_2 + a_2 v_1)$ where '$\wedge$' and '$< .|. >$' are the usual cross and dot products on $\mathbb{R}^3$

Moreover, we define the conjugate quaternion and the norm

- $\overline{(a, v)} = (-a, v)$
- $|q|^2 = \|q\|^2_{\mathcal{Q}} = \bar{q} * q = a^2 + \|v\|^2_{\mathbb{R}^3} = \|q\|^2_{\mathbb{R}^4}$

This allows to write very simply the inverse quaternion

$$q^{-1} = \frac{\bar{q}}{|q|^2}$$

for $q \neq 0$. We shall note that the norm is compatible with the product: $|q_1 q_2| = |q_1|.|q_2|$.

A more detailed introduction to quaternions and their properties is available in [Cas87] and [RA90].

## A.2 $\mathbb{R}^3$ Rotations

Among the linear maps of $\mathbb{R}^3$, vectorial rotations are the positive isometries (maps conserving orientation and dot product). With the composition law, this set forms a non-commutative group which can be represented as the set of $3 \times 3$ matrices on $\mathbb{R}$ verifying

$$R^t R = I \quad \text{and} \quad \det(R) = 1$$

A second representation, still non minimal, uses the quaternions (see section A.3. We can also use Euler's angles or the rotation vector [Aya91]. With the use of this last representation comes Rodrigues' formula : a rotation of angle $\theta$ around the unit vector $n$ is

$$R_{(n,\theta)} = I + \sin\theta\, \tilde{n} + (1 - \cos\theta)\tilde{n}^2$$

where the symbol $\sim$ denotes the operation which maps to a vector $n$ the skew matrix $\tilde{n}$ such as for all vector $v$ we have $\tilde{n}v = n_\wedge v$. If the coordinates of $n$ are $(n_x, n_y, n_z)$, the matrix $\tilde{n}$ is

$$\begin{pmatrix} 0 & -n_z & n_y \\ n_z & 0 & -n_x \\ -n_y & n_x & 0 \end{pmatrix}$$

## A.3 Quaternions and rotations

Let $q$ be a unit quaternion. Then there exists $\theta \in [0, \pi]$ and $n$ unit vector on $\mathbb{R}$ such that $q = \left(\cos\left(\frac{\theta}{2}\right), \sin\left(\frac{\theta}{2}\right).n\right)$. The map

$$\begin{array}{rccc} R_q : & \mathcal{Q} & \longrightarrow & \mathcal{Q} \\ & p & \longmapsto & q * p * \bar{q} \end{array}$$

is an inner automorphism of $\mathcal{Q}$ that conserves pure quaternions (null real part). Its restriction to $\mathbb{R}^3$ is the vectorial rotation of $\mathbb{R}^3$ with angle $\theta$ around the unit vector $n$. In a symmetric way, we can match to every rotation of $\mathbb{R}^3$ two unit quaternions $q$ and $-q$.

## A.4 Least squares minimization

Assuming we have a set of vectors $x_i$ and their supposed images $y_i$, we are looking for the vectorial rotation $R$ that minimizes the quadratic matching error between the $x_i$'s and the $y_i$'s. Therefore we want to minimize the criterion

$$C = \sum_i \|y_i - Rx_i\|^2$$

Noting $q$ one of the two unit quaternion associated with $R$ and identifying the $x_i$'s and the $y_i$'s to pure quaternions, we obtain

$$\begin{array}{rcl} C & = & \sum_i |y_i - q * x_i * \bar{q}|^2 \\ & = & \sum_i |y_i * q - q * x_i|^2 \\ & = & \sum_i [A_i.q]^t [A_i.q] \\ & = & q^t [\sum_i A_i^t A_i] q \\ & = & q^t B q \end{array}$$

if we note $A_i$ the $4 \times 4$ matrix verifying $A_i.q = y_i * q - q * x_i$ and $B = \sum_i A_i^t A_i$ . Using simple laws on quaternions, and writing the matrix in blocs

$$A_i = \begin{pmatrix} 0 & (y_i - x_i)^t \\ (y_i - x_i) & (\tilde{y_i} + \tilde{x_i}) \end{pmatrix}$$

$$A_i^t A_i = \begin{pmatrix} \|y_i - x_i\|^2 & (y_i - x_i)^t (\tilde{y_i} + \tilde{x_i}) \\ (\tilde{y_i} + \tilde{x_i})(x_i - y_i) & (y_i - x_i)(y_i - x_i)^t - (\tilde{y_i} + \tilde{x_i})^2 \end{pmatrix}$$

Developping terms and simplifying them thanks to Gibbs' formula[3] we obtain

$$A_i^t A_i = \begin{pmatrix} \|y_i - x_i\|^2 & 2(y_i \wedge x_i)^t \\ 2(y_i \wedge x_i) & \|y_i + x_i\|^2 I - 2(x_i y_i^t + y_i x_i^t) \end{pmatrix}$$

[3] $\tilde{a}\tilde{b} = ba^t - < a|b > I$

Hence we can write the matrix $B$

$$\begin{array}{l}\gamma = \sum(\|x_i\|^2 + \|y_i\|^2) \\ \alpha = \sum < x_i | y_i > \\ \beta = \sum x_i \wedge y_i \\ \Gamma = \sum(x_i y_i^t + y_i x_i^t)\end{array} \qquad B = \begin{pmatrix} \gamma - 2\alpha & -2\beta^t \\ -2\beta & (\gamma + 2\alpha)I - 2\Gamma \end{pmatrix} \qquad (1)$$

We wanted to minimize $C = q^t B q$ with the constraint $|q| = 1$: the answer is given by the unit eigenvector associated with the minimum eigenvalue of $B$. Unfortunately, if this resolution is well done numerically, we do not have a formal explicit solution.

## A.5 Superimposing two triplets of vectors in barycentric frame

Let us consider three vectors $x_i$ in barycentric coordinates, thus belonging to a plane $\mathcal{M}$ defined by its normal vector $m = (x_1 \wedge x_2)/\|x_1 \wedge x_2\|$, and their partners $y_i$, also in barycentric frame, belonging to the plane $\mathcal{S}$ defined par $s = (y_1 \wedge y_2)/\|y_1 \wedge y_2\|$.

Assuming the planes $\mathcal{M}$ and $\mathcal{S}$ are identical (the $x_i$'s and the $y_i$'s are coplanar) with the same orientation: $m = s$; we are going to find explicitly the least squares rotation. The analogy with the 2D case will help us proposing two rotation quaternions which we shall verify as being eigenvector of $B$. Some symmetry considerations will then allow us to find the two other eigenvalues of $B$, which will appear to be larger than the first. This will conclude our demonstration.

### A.5.1 $2 * 3$ vectors in two dimensions

The criterion to be minimized for the research of the vectorial rotation is

$$C = \sum_i \|y_i - R x_i\|^2 \quad \text{with} \quad R = \begin{pmatrix} \cos\theta & -\sin\theta \\ \sin\theta & \cos\theta \end{pmatrix}$$

To obtain optimal angles, we derivate $C$ with respect to $\theta$

$$\frac{\partial C}{\partial \theta} = 0 \quad \Leftrightarrow \quad \sin\theta \left\{ \sum_i < x_i | y_i > \right\} + \cos\theta \left\{ \sum_i |y_i, x_i| \right\} = 0$$

The solutions are then

$$\begin{cases} \cos\theta \sqrt{(\sum < x_i | y_i >)^2 + (\sum |y_i, x_i|)^2} = \pm \sum < x_i | y_i > \\ \sin\theta \sqrt{(\sum < x_i | y_i >)^2 + (\sum |y_i, x_i|)^2} = \sum |y_i, x_i| \end{cases}$$

Assume now the 6 vectors are in the 3D space, but coplanar. The 2D rotation we just proposed has an axis orthogonal to the plane. Calling $k$ the normal vector to the plane in the right handed way, we propose as rotation the quaternions (up to their norm)

$$q_1 = \left| \begin{array}{l} 1 + \cos\theta \\ \sin\theta . k \end{array} \right. \quad \text{and} \quad q_2 = \left| \begin{array}{l} 1 - \cos\theta \\ \sin\theta . k \end{array} \right.$$

which is with our notations

$$q_{1,2} = \left| \begin{array}{c} \sqrt{\alpha^2 + \|\beta\|^2} \pm \alpha \\ \beta \end{array} \right.$$

### A.5.2 Two eigenvectors for $B$

The verification of $q_1$ is

$$(B - \lambda I)q_1 = 0 \quad \Leftrightarrow \quad \left\{ \begin{array}{l} (\gamma - 2\alpha - \lambda)(\sqrt{\alpha^2 + \|\beta\|^2} + \alpha) = 2\|\beta\|^2 \\ \beta(\gamma - 2\sqrt{\alpha^2 + \|\beta\|^2} - \lambda) = 2\Gamma\beta \end{array} \right.$$

But $\beta = \sum x_i \wedge y_i$ is colinear to $m = s$ and thus orthogonal to the $x_i$'s and $y_i$'s, which proves that $\Gamma\beta = 0$. Thus we obtain

$$(B - \lambda_1 I)q_1 = 0 \quad \Leftrightarrow \quad \lambda_1 = \gamma - 2\sqrt{\alpha^2 + \|\beta\|^2}$$

As far as $q_2$ is concerned, we follow the same way and thus have

$$(B - \lambda_2 I)q_2 = 0 \quad \Leftrightarrow \quad \lambda_2 = \gamma + 2\sqrt{\alpha^2 + \|\beta\|^2}$$

Hence $q_1$ and $q_2$ are eigenvector of $B$ associated with the eigenvalues $\lambda_1$ and $\lambda_2$. We are now going to write them differently.

$$\begin{array}{rcl} \alpha^2 + \|\beta\|^2 & = & \left(\sum_i < x_i | y_i >\right)^2 + < \sum_i x_i \wedge y_i | \sum_i x_i \wedge y_i > \\ & = & \sum_{i,j} < x_i | y_i >< x_j | y_j > + \sum_{i,j} < x_i | x_j >< y_i | y_j > \\ & & - \sum_{i,j} < x_i | y_j >< x_j | y_i > \\ & = & \sum_{i,j} < x_i \wedge x_j | y_i \wedge y_j > + \sum_{i,j} < x_i | x_j >< y_i | y_j > \end{array}$$

Let $r$ be the second term. It does only rely on the relative position in between the $x_i$'s and in between the $y_i$'s. This value is thus invariant along the matching process, as $\gamma$ is. The first term simplifies a lot when we introduce the values of $x_3$ and $y_3$ in the barycentric frame: $x_3 = -x_1 - x_2$ and $y_3 = -y_1 - y_2$. Actually we obtain

$$\begin{array}{rl} \alpha^2 + \|\beta\|^2 & = r + 6 < x_1 \wedge x_2 | y_1 \wedge y_2 > \\ & = r + 6\|x_1 \wedge x_2\| . \|y_1 \wedge y_2\| < m | s > \end{array}$$

We didn't use the hypothesis $m = s$ in obtaining this expression, which is therefore always valid.

$$\alpha^2 + \|\beta\|^2 = r + 6\|x_1 \wedge x_2\| . \|y_1 \wedge y_2\| < m | s > \quad \text{with} \quad r = \sum_{i,j} < x_i | x_j >< y_i | y_j > \qquad (2)$$

Introducing this expression in our eigenvalues, we find a formula wich does not rely on the initial positions of $x_i$'s with regard to the $y_i$'s.

$$\lambda_{1,2} = \gamma \mp 2\sqrt{r + 6\|x_1 \wedge x_2\| . \|y_1 \wedge y_2\|}$$

### A.5.3 The two other eigenvalues

Let $\mu_1$ and $\mu_2$ be the two eigenvalues of $\Gamma$ if they do exist, and $n_1, n_2$ the two associated unit eigenvector. According to the very formulation of $\Gamma$, they are in $\mathcal{M} = \mathcal{S}$. We easily verify that $q_{3,4} = \left| \begin{array}{l} 0 \\ n_{3,4} \end{array} \right.$ is eigenvector of $B$ associated with the eigenvalue $\lambda_{3,4} = \gamma + 2\alpha - \mu_{3,4}$. But $q_3$ and $q_4$ correspond to rotations of angle $\pi$ around an axis belonging to the plane $\mathcal{M} = \mathcal{S}$: they are symmetries with respect to lines for this plane. We can then retrieve the eigenvalues $\lambda_3$ and $\lambda_4$ in focusing on the rotations of axis $m$ (or $s$) in the case $m = -s$. The reasoning used to find $\lambda_1$ and $\lambda_2$ taking into account only $\beta \,//\, m \,//\, s$, we find

$$\lambda_{3,4} = \gamma \pm 2\sqrt{\alpha^2 + ||\beta||^2}$$

Taking into account $< m|s >= -1$ in equation 2, this writes

$$\lambda_{3,4} = \gamma \mp 2\sqrt{r - 6||x_{1\wedge}x_2||.||y_{1\wedge}y_2||}$$

### A.5.4 Conclusion

For all initial position of the $x_i$'s with regard to the $y_i$'s, we can decompose the rotation $A$, minimizing the least squares error, into a rotation $A_1$ that superimposes vector $m$ on vector $s$, then a rotation $A_2$ which satisfies the constraints we just developed. The eigenvalues being written in an invariant form for rotations on the $x_i$'s, they are still valid.

**Theorem 5** *The eigenvalues of matrix $B$ are*

$$\begin{array}{ll} \lambda_1 = \gamma - 2\sqrt{r + 6||x_{1\wedge}x_2||.||y_{1\wedge}y_2||} & \lambda_2 = \gamma + 2\sqrt{r + 6||x_{1\wedge}x_2||.||y_{1\wedge}y_2||} \\ \lambda_3 = \gamma - 2\sqrt{r - 6||x_{1\wedge}x_2||.||y_{1\wedge}y_2||} & \lambda_4 = \gamma + 2\sqrt{r - 6||x_{1\wedge}x_2||.||y_{1\wedge}y_2||} \end{array}$$

*with the notations*

$$\gamma = \sum_{i=1}^{3} (||x_i|| + ||y_i||) \qquad r = \sum_{i=1,j=1}^{3,3} < x_i|x_j >< y_i|y_j >$$

*The order is $\lambda_1 \leq \lambda_3 \leq \lambda_4 \leq \lambda_2$. The criterion value is thus minimal for $\lambda_1$, and the researched quaternion is the unit eigenvector associated with this value.*

The rotations superimposing $m$ and $s$ are linear combination (up to the norm) of

$$p_1 = \left| \begin{array}{l} 1 + < m|s > \\ m_{\wedge}s \end{array} \right. \qquad p_2 = \left| \begin{array}{l} 0 \\ m + s \end{array} \right.$$

There is however a singularity in $m = -s$, which we exploited before, and for which this is not valid. In this case, any rotation of angle $\pi$ with an axis in the plane suits.
Except this singularity, the rotation with the minimal angular value is given by $p_1$. Let's note $R_1$ the equivalent rotation and $x'_i = R_1 x_i$. The rotation $R_2$ leading to the minimum of $C$ is then given by

$$q_1 = \left| \begin{array}{l} \sqrt{\alpha'^2 + ||\beta'||^2} + \alpha' \\ \beta' \end{array} \right. \quad \text{with} \quad \begin{array}{l} \alpha' = \sum_{i=1}^{3} < x'_i|y_i > \\ \beta' = \sum_{i=1}^{3} x'_{i\wedge}y_i \end{array}$$

**Corollary 1** *It is always possible to decompose the sought rotation $R$ into $R = R_2R_1$ where $R_1$ is a rotation superimposing $m$ and $s$, and $R_2$ is a rotation of axis $s$.*

# B Computing the rotational error

Assuming we have a method to compute a rotation from data. Let $R$ let the one computed on exact data and $\bar{R}$ the one on disturbed data. $\bar{R}$ can be considered as the composition of the exact rotation $R$ followed by an adjustment rotation $\Gamma$ : $\bar{R} = \Gamma R$. The rotational error is then $\delta R = (\Gamma - I_d)R$ and its norm $\|\delta R\| = \|\Gamma - I_d\|$. Thus, $\|\delta R\|$ is independent of $R$: without loss of generality we will assume that $R = I_d$ in this section. Let $\theta$ be the angular value of the adjustment rotation and $r$ the unit vector supporting this axis. Using Rodrigues's formula (see appendix A) we have

$$\delta R = \bar{R} - I_d = \sin\theta\, \tilde{r} + (1 - \cos\theta)\tilde{r}^2$$

$$\begin{aligned} \|\delta R\, x\|^2 &= \|(\sin\theta)\, r_\wedge x + (1 - \cos\theta)\, r_\wedge(r_\wedge x)\|^2 \\ &= \sin^2\theta \|x\|^2 \sin^2(\widehat{r,x}) + (1 - \cos\theta)^2 \|x\|^2 \sin^2(\widehat{r,x}) \end{aligned}$$

By definition we have $\|\delta R\| = \max_{\|x\|=1} \|\delta R x\|$ hence we find

**Lemma 5** *Let $\theta$ be the angular value of the rotation $\Gamma = \bar{R}R^{-1}$. We have*

$$\|\delta R\| = \sqrt{2}\sqrt{1 - \cos\theta} = \theta + O(\theta^3)$$

### B.0.5 Composing rotations

In the following parts of this section, we will have to use a small lemma concerning the composition of two rotations with orthogonal axes which proves that we can independently consider each rotation and combine afterward their result :

**Lemma 6** *Let $R$ be a rotation with rotational vector $\theta r$ which can be decomposed into two rotations $R_1$ and $R_2$ with rotational vectors $\theta_1 r_1$ and $\theta_2 r_2$. Up to the first order, we have*

$$R = R_2 R_1 = R_1 R_2 + O(\theta^2) = R_1 + R_2 - I_d + O(\theta^2)$$

*The two rotations $R_1$ and $R_2$ can then be independently determined, their combination result being given by*

$$\theta r = \theta_1 r_1 + \theta_2 r_2 + O(\theta^2)$$

*Moreover, assuming $r_1$ is orthogonal to $r_2$*

$$\theta = \sqrt{\theta_1^2 + \theta_2^2} + O(\theta^2)$$

Indeed, using first order limited development on Rodrigues's formula

$$\forall x \quad R\, x = \theta\, r_\wedge x + O(\theta^2) = \theta_1\, r_{1\wedge} x + \theta_2\, r_{2\wedge} x + O(\theta^2)$$

$$\forall x \quad (\theta\, r - \theta_1\, r_1 + \theta_2\, r_2)_\wedge x + O(\theta^2) = 0$$

$$\theta\, r = \theta_1\, r_1 + \theta_2\, r_2 + O(\theta^2)$$

Since $\theta$ is always positive, $r_1$ being orthogonal to $r_2$ implies that $\theta = \|\theta\, r\| = \sqrt{\theta_1^2 + \theta_2^2} + O(\theta^2)$

### B.0.6 Using barycentric coordinates

For both methods we study at section 2, we take the origins at the barycenter of each minimal set. Using these baricentric coordinates, the rotation $R$ maps exactly the $x_i$'s on the $y_i$'s, and $\bar{R}$ maps approximately the $x_i$'s on the $\bar{y}_i$'s. Since we take $R = I_d$, we have $x_i = y_i$. We will preferably use the $y_i$ notation to recall the elimination of the rotation $R$, except when it comes to speaking of invariants.

For ease of work, we compute now the propagated error on barycentric coordinates. We have for example

$$\|\delta y_1\| = \|\frac{2}{3}\delta s_1 - \frac{1}{3}\delta s_2 - \frac{1}{3}\delta s_3\| \leq \frac{4}{3}\varepsilon_p$$

It is easy to see that for each point in the minimal set the computation is the same : $\|\delta y_i\| \leq \varepsilon_y = \frac{4}{3}\varepsilon_p$

## B.1 Error for the least squares method

### B.1.1 Decomposition of the adjustment rotation $\bar{R}$

Using barycentric coordinates, the three points $y_i$ define a vectorial plane $\mathcal{P}$ and the three $\bar{y}_i$ a plane $\bar{\mathcal{P}}$. We can describe entirely those vectorial planes by the normal vectors $n = y_{1\wedge}y_2$ and $\bar{n} = \bar{y}_{1\wedge}\bar{y}_2$ (which are noted $m$ and $s$ in appendix A.5). Assume $R_1$ is the rotation of axis $r_1 = \frac{n\wedge\bar{n}}{\|n\wedge\bar{n}\|}$ and angle $\theta_1 = (\widehat{n,\bar{n}})$: it maps the $\mathcal{P}$ plane on the $\bar{\mathcal{P}}$ plane. Let's now decompose $\bar{R}$ in $\bar{R} = R_2\,R_1$. From corollary 1 (appendix A.5), $R_2$ is a rotation of axis $\bar{n}$. Let's note $(r_2 = \frac{\bar{n}}{\|\bar{n}\|}, \theta_2)$ its parameters. Since $\bar{R}$ is an adjustment rotation, we will assume that every angular value is small and therefore apply lemma 6 : we will independently bound the angles $\theta_1$ and $\theta_2$, and combining the results with lemma 5, the result will be

**Lemma 7** *Assuming the angle of adjustment rotation $\theta$ is small, and using previous notations, the rotational error for the least squares method is*

$$\|\delta R\| = \sqrt{\theta_1^2 + \theta_2^2} + O(\theta^2)$$

### B.1.2 Bounding $\theta_1$

Since we are in barycentric frame, we have $n = y_{1\wedge}y_2 = y_{2\wedge}y_3 = y_{3\wedge}y_1$ and $\bar{n} = \bar{y}_{1\wedge}\bar{y}_2 = \bar{y}_{2\wedge}\bar{y}_3 = \bar{y}_{3\wedge}\bar{y}_1$
Developing $\bar{y}_i = y_i + \delta y_i$ we can write

$$\bar{n} = n + \frac{1}{3}\left((y_3 - y_2)_\wedge \delta y_1 + (y_1 - y_3)_\wedge \delta y_2 + (y_2 - y_1)_\wedge \delta y_3\right) + O({\varepsilon_y}^2)$$

$$\bar{n} = n + \delta n \qquad \text{with} \qquad \|\delta n\| \leq \frac{\varepsilon_y}{3}\left(\sum_{i<j}\|x_i - x_j\|\right) + O({\varepsilon_y}^2)$$

It is therefore easy to see that the maximum angle $\theta_1^{max}$ is obtained in the case of figure 9, and we obtain $\sin\theta_1^{max} = \varepsilon_y \left(\sum_{i<j}\|x_i - x_j\|\right) / \left(3\,\|x_{1\wedge}x_2\|\right) + O(\varepsilon_y^2)$

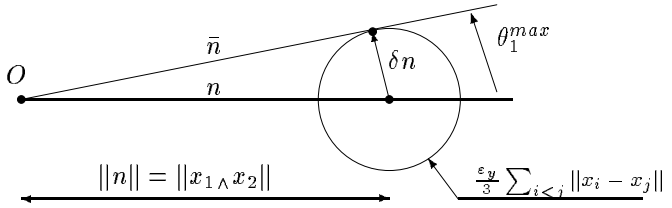


Figure 9: Maximum angular value for the rotation $R_1$

**Lemma 8** *Using previous notations, the maximum angular value $\theta_1^{max}$ of the rotation $R_1$ is given by*

$$\theta_1^{max} = \frac{4}{9}\varepsilon_p \frac{\sum_{i<j}\|x_i - x_j\|}{\|x_{1\wedge}x_2\|} + O(\varepsilon_p^2)$$

### B.1.3 Bounding $\theta_2$

when using the method based on quaternions to solve for the rotation, we have no information on the angular value of this second rotation. Hence, we will use a direct minimization for the limited development of the criterion. Examining first the effect of the two rotations $R_1$ and $R_2$

$$R\,x = R_2R_1\,x = I + \theta_1 r_{1\wedge}x + \theta_2 r_{2\wedge}x + O(\theta^2)$$

and recalling that for the analysis $x_i = y_i$, we can rewrite the criterion

$$C = \sum \|\delta y_i - \theta_1.r_{1\wedge}y_i - \theta_2.r_{2\wedge}y_i\|^2 + O(\theta^3)$$

Since by definition $n$ is orthogonal to each $y_i$, $\left(\frac{y_i}{\|y_i\|}; \frac{n}{\|n\|}; \frac{y_{i\wedge}n}{\|y_i\|\,\|n\|}\right)$ is an orthonormal frame and we can decompose each $\delta y_i$ in three terms bounded by $\varepsilon_y$

$$\delta y_i = (\delta y_i)_y \frac{y_i}{\|y_i\|} + (\delta y_i)_n \frac{n}{\|n\|} + (\delta y_i)_t \frac{y_{i\wedge}n}{\|y_i\|\,\|n\|}$$

On the other hand, $r_{1\wedge}y_i = \frac{(n_\wedge\bar{n})_\wedge y_i}{\|n_\wedge\bar{n}\|} = -\frac{<y_i|\bar{n}>}{\|n_\wedge\bar{n}\|}n$ by Gibbs formula, and $r_{2\wedge}y_i = \frac{\bar{n}_\wedge y_i}{\|\bar{n}\|} = \frac{n_\wedge y_i}{\|n\|} + O(\theta)$. Therefore, we can split each term into three in the criterion :

$$C = \sum(\delta y_i)_y^2 + \sum\left((\delta y_i)_t + \theta_2\|y_i\|\right)^2 + \sum\left((\delta y_i)_n + \theta_1\frac{<y_i|\bar{n}>}{\|n_\wedge\bar{n}\|}\|n\|\right)^2 + O(\theta^3)$$

The minimum in $\theta_2$ is obtained in taking the derivative according to this variable

$$\frac{\partial C}{\partial\theta_2} = 2\sum\|x_i\|\left((\delta y_i)_t - \theta_2\|x_i\|\right) + O(\theta^2) = 0 \quad \Leftrightarrow \quad \theta_2 = \frac{\sum\|x_i\|(\delta y_i)_t}{\sum\|x_i\|^2} + O(\theta^2)$$

Taking the bound $\varepsilon_y$ on $(\delta y_i)_t$ we got the result.

**Lemma 9** *Using previous notations, the maximum angular value $\theta_2^{max}$ of the rotation $R_2$ is given by*

$$\theta_2^{max} = \frac{4}{3}\varepsilon_p \frac{\sum \|x_i\|}{\sum \|x_i\|^2} + O({\varepsilon_p}^2)$$

**Theorem 6** *Computing the least squares rigid transformation between a model and a scene minimal set, the rotational error is bounded by*

$$\|\delta R\| \leq \frac{4\,\varepsilon_p}{3}\sqrt{\frac{\left(\sum_{i<j}\|x_i - x_j\|\right)^2}{9\,\|x_{1\wedge}x_2\|^2} + \frac{\left(\sum \|x_i\|\right)^2}{\left(\sum \|x_i\|^2\right)^2}} + O\left({\varepsilon_p}^2\right)$$

*where the $x_i$'s are the barycentric coordinates of the three points of the model minimal set.*

## B.2 Error for the basis definition method

We now have to bound $\|\delta R_{rec}\|$ as defined in the section 2.3. Lemma 5 once again shows us that we can do it in the special case where $R_{rec} = I_d$. The rotation $\bar{R}_{rec}$ is thus simply the rotation between the basis defined from $(y_1, y_2, y_3)$, which is the canonical basis, and the basis defined by $(\bar{y}_1, \bar{y}_2, \bar{y}_3)$. Using previous notations, the first axis of those bases are according to section 2.3 $\frac{y_{1\wedge}y_2}{\|y_{1\wedge}y_2\|} = \frac{n}{\|n\|}$ and $\frac{\bar{y}_{1\wedge}\bar{y}_2}{\|\bar{y}_{1\wedge}\bar{y}_2\|} = \frac{\bar{n}}{\|\bar{n}\|}$, and the second axis are in the planes $\mathcal{P}$ and $\bar{\mathcal{P}}$.

As in the least squares case, we can decompose the rotation $\bar{R}_{rec}$ in $\bar{R}_{rec} = R'_2\,R'_1$ where $R'_1$ is in fact exactly the same as $R_1$ in the previous section, and $R'_2$ is of axis $\bar{n}$. Hence, we can once again apply the results of lemma 6, and moreover, lemma 8 still holds. We just have to compute a bound on the angular value $\theta'_2$ of $R'_2$, and we can do as if it were the first rotation.

In this case, $\theta'_2$ is simply the angular value between $e_2$ and $\bar{e}_2$. With the order convention, we have $e_2 = y_2 - y_1 = s_2 - s_1$ and $\bar{e}_2 = \bar{y}_2 - \bar{y}_1 = s_2 - s_1 + \delta s_2 - \delta s_1$. Therefore, $\bar{e}_2 = e_2 + \delta e_2$ with $\|\delta e_2\| \leq 2\,\varepsilon_p$, and the maximum value $\theta_{2'}^{max}$ is given as in section B.1.2 by

$$\theta_{2'}^{max} = \frac{2\varepsilon_p}{\|e_2\|} + O(\varepsilon_p^2) = \frac{2\varepsilon_p}{\|x_2 - x_1\|} + O(\varepsilon_p^2) = \frac{2\varepsilon_p}{\max_{i,j}\|x_i - x_j\|} + O(\varepsilon_p^2)$$

**Theorem 7** *Computing the rigid transformation between a model and a scene minimal set by the basis definition method (or the coordinates of a scene point in the scene basis), the rotational error is bounded by*

$$\|\delta R_{rec}\| \leq \frac{4\,\varepsilon_p}{3}\sqrt{\frac{\left(\sum_{i<j}\|x_i - x_j\|\right)^2}{9\,\|x_{1\wedge}x_2\|^2} + \frac{9}{4\,\max_{i,j}\|x_i - x_j\|^2}} + O\left({\varepsilon_p}^2\right)$$

*where the $x_i$'s are the barycentric coordinates of the three points of the model minimal set.*

# References

[AF86] N. Ayache and O.D. Faugeras. Hyper : A new approach for the recognition and positionning of two-dimensionnal objects. *IEEE Trans. on Patern Analysis and Machine Intelligence*, 8(1):44–54, 1986.

[AG93] T.D. Alter and W.E.L Grimson. Fast and robust 3d recognition by alignment. In *Proceedings of Int. Conf on Comput. Vis. and Pat. Recog*, pages 113–120, IEEE Computer Society Press, 1993.

[Aya91] N. Ayache. *Artificial Vision for Mobile robots - Stereo-vision and Multisensor Perception.* MIT-Press, 1991.

[Aya93] N. Ayache. Computer vision applied to 3d medical images: Results, trends and future challenges. In *Int. Symp. on Robotic Research, Hidden Valley, Pensylvania, USA*, 1993. Also as INRIA Research Report No 2050.

[Ber92] M. Berger. *Géométrie.* Volume 1, Nathan, 1992.

[Cas87] P. Casteljau. *Les quaternions.* Hermes, 1987.

[Dan80] P.E. Danielsson. Euclidean distance mapping. *Comp. Journ. of Image Processing*, 14:227–248, 1980.

[GA92] A. Guéziec and N. Ayache. Smoothing and matching of 3d space curves. In *Proceedings of the Second European Conference on Computer Vision*, Santa Margherita Ligure, Italy, 1992.

[GA93] A. Guéziec and N. Ayache. New develoments on geometric hashing for matching 3d curves. In *Proceedings of Int. Conf on Comput. Vis. and Pat. Recog*, pages 703–704, IEEE Computer Society Press, 1993.

[GH90] W.E.L. Grimson and D.P. Huttenlocher. On the sensitivity of geometric hashing. In *Proc. third ICCV*, pages 334–338, 1990.

[GHJ93] W.E.L. Grimson, D.P. Huttenlocher, and D.W Jacobs. A study of affine matching with bounded sensor error. 1993. to appear in Int. Journ. of Comput. Vision.

[Gri92] W.E.L. Grimson. *Object Recognition by Computer - The role of Geometric Constraints.* MIT Press, 1992.

[HU87] D.P. Huttenlocher and S. Ullman. Object recognition using alignement. In *Proc. of ICCV*, pages 72–78, 1987.

[LW88] Y. Lamdan and H.J. Wolfson. Geometric hashing : A general and efficiant model-based recognition scheme. In *Proc. of Second ICCV*, pages 238–289, 1988.

[LW91] Y Lamdan and H.J. Wolfson. On the error analysis of geometric hashing. In *IEEE Int. Conf. on Comput. Vis. and Patt. Recog.*, pages 22–27, 1991.

[RA90] L. Reyes-Avila. *Les quaternions : une représentation paramétrique systématique des rotations finies.* Rapport de Recherche 1303, INRIA, 1990.

[RH91a] I. Rigoutsos and R. Hummel. Several results on affine invariant geometric hashing. In *Proc. 8th Israeli Conf. on Artificial Intelligence and Computer Vision*, pages 1–12, 1991.

[RH91b] I. Rigoutsos and R. Hummel. Robust similarity invariant matching in the presence of noise. In *Proc. 8th Israeli Conf. on Artificial Intelligence and Computer Vision*, pages 27–43, 1991.

[RH93] I. Rigoutsos and R. Hummel. Distributed bayesian object recognition. In *Proceedings of Int. Conf on Comput. Vis. and Pat. Recog*, pages 180–186, IEEE Computer Society Press, 1993.

[Rig92] I Rigoutsos. *Massively Parallel Baysian Object Recognition.* Ph.D. dissertation, New York University, 1992.

[SG93] K.B. Sarachik and W.E.L. Grimson. Gaussien error models for object recognition. In *Proceedings of Int. Conf on Comput. Vis. and Pat. Recog*, pages 400–406, IEEE Computer Society Press, 1993.

[TB93] J.P. Thirion and S. Benayoun. *Image Surface Extremal Points, new feature points for Image Registration.* Research Report 2003, INRIA, 1993.

[TG93] J.P. Thirion and A. Gourdon. *The marching lines algorithm : new results and proofs.* Research Report 1881, INRIA, 1993. submitted to CVGIP.

[TGMG92] J.P. Thirion, A. Gourdon, O. Monga, A. Gueziec, and N. Ayache. Automatic registration of 3d cat-scan images using surface curvature. In *14th Ann. Int. Conf. of the IEEE EMBS satellite symposium on 3D Advanced Image Processing in Medecine - Rennes*, pages 85–90, 1992.

[Thi93] J.P. Thirion. *New Feature Points based on geometric invariants for 3D Image Registration.* Research Report 1901, INRIA, 1993.

[Tsa93] F.C. Tsai. *A Probabilistic Approach to Geometric Hashing using Line Feature.* Technical Report 640, Robotic Research Laboratory, Courant Institute of Mathematical Science, N.Y. Univ., 1993.

[Wol90] H.J. Wolfson. Model-based recognition by geometric hashing. In O. Faugeras, editor, *Proc. of 1st Europ. Conf. on Comput. Vision (ECCV 90)*, pages 526–536, Springer-Verlag, 1990. Lecture Note in Computer Science 427.

Unité de recherche INRIA Lorraine, Technôpole de Nancy-Brabois, Campus scientifique,
615 rue de Jardin Botanique, BP 101, 54600 VILLERS LÈS NANCY
Unité de recherche INRIA Rennes, IRISA, Campus universitaire de Beaulieu, 35042 RENNES Cedex
Unité de recherche INRIA Rhône-Alpes, 46 avenue Félix Viallet, 38031 GRENOBLE Cedex 1
Unité de recherche INRIA Rocquencourt, Domaine de Voluceau, Rocquencourt, BP 105, 78153 LE CHESNAY Cedex
Unité de recherche INRIA Sophia-Antipolis, 2004 route des Lucioles, BP 93, 06902 SOPHIA-ANTIPOLIS Cedex

Éditeur
INRIA, Domaine de Voluceau, Rocquencourt, BP 105, 78153 LE CHESNAY Cedex (France)
ISSN 0249-6399